



Nanoscale

**Self-assembled HfO<sub>2</sub>-Au nanocomposites with ultra-fine vertically aligned Au nanopillars**

Journal:	<i>Nanoscale</i>
Manuscript ID	NR-ART-06-2022-003104.R1
Article Type:	Paper
Date Submitted by the Author:	12-Jul-2022
Complete List of Authors:	Zhang, Yizhi; Purdue University, MSE Zhang, Di; Purdue University, Materials Engineering; Los Alamos National Laboratory, Center for Integrated Nanotechnologies Liu, Juncheng; Purdue University Lu, Ping; Sandia National Laboratories, Deitz, Julia; Sandia National Laboratories Shen, Jianan; Purdue University System, MSE He, Zihao; Purdue University Zhang, Xinghang; Purdue University System, Materials Engineering Wang, Haiyan; Purdue University System, MSE; Neil Armstrong Engineering Building

SCHOLARONE™  
Manuscripts

# **Self-assembled HfO<sub>2</sub>-Au nanocomposites with ultra-fine vertically aligned Au nanopillars**

Yizhi Zhang,<sup>1</sup> Di Zhang,<sup>2</sup> Juncheng Liu,<sup>1</sup> Ping Lu,<sup>3</sup> Julia Deitz,<sup>3</sup> Jianan Shen,<sup>1</sup> Zihao He,<sup>1</sup> Xinghang Zhang,<sup>1</sup> Haiyan Wang<sup>1,4\*</sup>

<sup>1</sup> *School of materials engineering, Purdue University, West Lafayette, 47907, USA*

<sup>2</sup> *Los Alamos National Laboratory, Los Alamos, NM 87545, USA*

<sup>3</sup> *Sandia National Laboratories, Albuquerque, NM 87185, USA*

<sup>4</sup> *School of Electrical and Computer Engineering, Purdue University, West Lafayette, 47907, USA*

\*Address correspondence to: [hwang00@purdue.edu](mailto:hwang00@purdue.edu) (Haiyan Wang)

## Abstract

Oxide-metal-based hybrid materials have gained great research interest in recent years owing to their potential towards multifunctionality, property coupling, and tunability. Specifically, oxide-metal hybrid materials in a vertically aligned nanocomposite (VAN) form could produce pronounced anisotropic physical properties, e.g., hyperbolic optical properties. Herein, self-assembled HfO<sub>2</sub>-Au nanocomposites with ultra-fine vertically aligned Au nanopillars (as fine as 3 nm in diameter) embedded in a HfO<sub>2</sub> matrix were fabricated using a one-step self-assembly process. The film crystallinity and pillar uniformity can be obviously improved by adding an ultra-thin TiN-Au buffer layer during the growth. The HfO<sub>2</sub>-Au hybrid VAN films show an obvious plasmonic resonance at 480 nm, which is much lower than the typical plasmonic resonance wavelength of Au nanostructures, and is attributed to the well aligned ultra-fine Au nanopillars. Coupled with the broad hyperbolic dispersion ranging from 1050 nm to 1800 nm in wavelength, and unique dielectric HfO<sub>2</sub>, this nanoscale hybrid plasmonic metamaterial present strong potentials for future integrated optical and electronic switching device designs.

**Key words:** Oxide-metal VAN, metamaterials, PLD, anisotropic, plasmonic

## Introduction

Metamaterials are artificial materials that display extraordinary optical, electrical, and mechanical properties that are difficult to achieve in natural materials.<sup>1, 2, 3, 4</sup> The metamaterials' unique properties make them valuable for applications in various fields, including chemical catalysis<sup>5, 6</sup>, optics<sup>7</sup>, and sensors<sup>8</sup>. Recently significant work has been focused on enabling multifunctionality and tunability of these metamaterials.<sup>9, 10</sup> One class of metamaterials is highly anisotropic materials which present hyperbolic optical properties.<sup>11</sup> In these metamaterials, the signs of the permittivity ( $\epsilon$ ) are opposite along in-plane (IP) and out-of-plane (OP) directions, leading to some extraordinary optical responses that have great potential in various fields such as physical research<sup>12</sup>, subwavelength resolution imaging, photocatalysis, superlens, cloaking.<sup>13, 14, 15, 16</sup>

Various methods have been demonstrated for the fabrication of anisotropic metamaterials, including e-beam lithography<sup>17</sup>, membrane projection lithography<sup>18</sup>, chemical method<sup>19, 20</sup>, electrodeposition<sup>21</sup>, chemical vapor deposition (CVD)<sup>22</sup>, and physical vapor deposition (PVD)<sup>23</sup>. Recently, pulsed laser deposition (PLD) has shown its unique advantages in fabricating complex two-phase or three-phase nanocomposite thin films<sup>24, 25, 26</sup>, especially for the growth of oxide-metal vertically aligned nanocomposites (VAN)<sup>7, 27</sup>. VAN thin films typically consist of one phase as nanopillars embedded in the matrix phase, and show intriguing optical<sup>28</sup>, magnetic<sup>29</sup>, ferroelectric, and multiferroic properties<sup>30</sup>, taking advantage of their unique vertical interface coupling. The VAN hybrid structures can generate strong anisotropy compared to pure phase thin films, which makes them strong candidates for hybrid

hyperbolic metamaterials. Several oxide-metal VAN systems with interesting optical properties have been successfully integrated, such as tunable localized surface plasmon resonance (LSPR) peak in the visible and near-infrared regimes in BaTiO<sub>3</sub>-Au VANs<sup>31</sup>, hyperbolic property for near-field electromagnetic wave manipulation in La<sub>0.67</sub>Sr<sub>0.33</sub>MnO<sub>3</sub>-Au VANs<sup>7</sup>, and highly anisotropic and hyperbolic optical response in ZnO-Cu VAN systems<sup>32</sup>. Most of the Au nanostructures reported in VAN hybrid systems are Au nanopillars with the diameter ranging from 5 nm to 25 nm and plasmonic resonance response ranging from 550 nm to 600 nm.<sup>33, 34, 35</sup> The nanopillars grow epitaxially with morphology tunability achieved by tuning laser frequency, oxygen partial pressure<sup>36</sup>, metal composition<sup>7</sup>, film growth thickness<sup>2</sup>, and alloying with other metals<sup>37, 38, 39</sup>.

In this work, we demonstrate the growth of self-assembled HfO<sub>2</sub>-Au VAN hybrid metamaterials fabricated using PLD. HfO<sub>2</sub> is selected as the dielectric matrix material considering its high refractive index for its broad applications as anti-reflection coatings, bandpass filters, beam splitters, and high reflectivity mirrors<sup>40, 41, 42</sup>, and its high-k dielectric nature for broad applications in semiconductor industry. On the other hand, Au is a plasmonic material and presents broad applications in optics. Additionally, Au is a noble metal and an ideal candidate for integration in a HfO<sub>2</sub>-based oxide-metal hybrid system. SrTiO<sub>3</sub> (a=3.905 Å) substrate was used for the nanocomposite deposition. HfO<sub>2</sub> has multiple polymorphs including cubic, monoclinic, tetragonal and orthorhombic structures, with lattice parameters ranging from 3.26 nm to 6.39 nm, and all dielectric materials. As shown in Fig. 1, besides the direct growth of HfO<sub>2</sub>-Au VAN,

we also implemented a seed layer of TiN-Au (TiN,  $a=4.249$  Å) for facilitating the nucleation and growth of the Au nanopillars, and to reduce the strain between thin films and the substrate. We compared the crystallinity and optical properties of the composite film with and without the seed layer for exploring the seed layer growth effects in this system.

## **Experimental details**

### **Thin film growth**

The self-assembled thin films were deposited under vacuum using pulsed laser deposition (with a KrF excimer laser,  $\lambda=248$  nm). The buffered HfO<sub>2</sub>-Au thin film was fabricated with a two-step growth using a TiN-Au buffer layer as a template. Firstly, TiN-Au layer was directly deposited on the single crystal STO (001) substrate with a TiN target. Then the HfO<sub>2</sub>-Au layer was deposited on the top of the TiN-Au buffer layer with a HfN/Au target. As for the unbuffered HfO<sub>2</sub>-Au thin film, the HfO<sub>2</sub>-Au layer was directly deposited on the single crystal STO (001) substrate under the same condition. All the films were deposited under vacuum at the temperature of 600 °C.

### **Structure and optical characterization**

The microstructure of the films was characterized using X-ray diffraction (XRD, PANalytical Empyrean), Transmission Electron Microscopy (TEM), and Scanning Transmission Electron Microscopy (STEM) (FEI TALOS 200X operated at 200 kV, and FEI Titan<sup>TM</sup> G2 80-200 STEM with a Cs probe corrector and ChemiSTEM<sup>TM</sup> technology, operated at 200 kV), and STEM electron-dispersive X-ray spectroscopy

(EDS). STEM images were taken with a high-angle annular dark-field (HAADF) detector with a collection range of 60-160 mrad. The dielectric permittivity of the films was measured using a spectroscopic ellipsometer (JA Woollam RC2). The obtained data was modeled as in-plane ( $\epsilon^{\parallel}$ ) and out-of-plane ( $\epsilon^{\perp}$ ) components using the general oscillator models to make them Kramers–Kronig consistent. The transmittance of the films was measured using Lambda 1050 with 3D detector (normal beam test) and total absolute measurement system (TAMS) detector (different incident angle test).

## Results and discussion

### 2.1 Structural analysis of the HfO<sub>2</sub>-Au films by XRD

The crystallinity of the thin films was characterized using  $\theta$ - $2\theta$  XRD scans first. Fig. 1 show the  $\theta$ - $2\theta$  XRD scans of the composite films with and without TiN-Au buffer layer. For the composite film with a TiN-Au buffer layer, a peak of  $34.04^{\circ}$  is visible, indexed as the monoclinic HfO<sub>2</sub> ( $002$ ), indicating a preferred ( $001$ ) orientation of HfO<sub>2</sub>. According to the PDF #43-1017 for the HfO<sub>2</sub>, the peak at  $2\theta = 34.04^{\circ}$  corresponds to a d-spacing of 5.263 Å, which is slightly larger than the d-spacing of 5.216 Å of the bulk counterpart (or standard  $2\theta = 34.357^{\circ}$ ). This result suggests a tensile strain in the out-of-plane direction for HfO<sub>2</sub>, which is caused by the lattice mismatch between the film and the substrate, as well as the strain between pillars and matrix. Clearly visible are TiN ( $200$ ) at  $42.86^{\circ}$ , Au ( $200$ ) at  $44.42^{\circ}$  and Au ( $220$ ) at  $64.97^{\circ}$ . In comparison, only STO ( $100$ ) peaks could be clearly identified from the sample without the buffer layer, indicating poor crystal quality (i.e., much smaller grain size) and polycrystalline

nature of the composite film. Since the XRD tool was set for epitaxial peak identification, the peaks from films with poor crystal quality can be very weak. It is noted that the film diffractions can be observed under TEM diffraction mode and will be discussed later. This poor crystal quality is likely due to the large lattice mismatch between  $\text{HfO}_2$  and STO. In short, the XRD results demonstrate that the crystallinity of the  $\text{HfO}_2$ -Au thin film is improved by applying the TiN-Au buffer layer.

It is noted that the presence of  $\text{HfO}_2$  peak indicates the oxidation of HfN during the PLD process. (As shown in Fig. S1, the target used for deposition is a pure HfN target). To better understand the oxidation process during the deposition, a pure HfN sample was fabricated with the same HfN target under the same growth condition. As shown in Fig. S2, the pure HfN film can be obtained with HfN target only, while the HfN-Au co-growth led to the formation of  $\text{HfO}_2$ -Au film. It is believed that Au could assist the conversion of HfN to  $\text{HfO}_2$  during the PLD growth despite the high base vacuum of  $10^{-7}$  Torr achieved prior to the deposition.

## 2.2 Morphology of the $\text{HfO}_2$ -Au VANs by TEM/STEM

TEM and STEM coupled with EDS analysis was conducted to further characterize the microstructure of the thin films. The cross-sectional HAADF STEM image of  $\text{HfO}_2$ -Au film on STO without buffer is shown in Fig. 3a along with the schematic diagram in Fig. 3b. The total film thickness is around 60 nm. Both Au pillars and Au particles are randomly distributed inside the  $\text{HfO}_2$  matrix, with short and discontinued pillars. The selected area electron diffraction (SAED) pattern in Fig. 3f indicates that the  $\text{HfO}_2$



matrix is polycrystalline with several growth orientations. In comparison, the morphology and growth quality of HfO<sub>2</sub>-Au film was significantly improved after including the TiN-Au buffer layer (Fig. 3d). The VAN structure also became more ordered which is similar to the schematic drawing in Fig. 3c. Specifically, the ultra-thin Au pillars are well aligned and embedded in the HfO<sub>2</sub> matrix and grew straight throughout the entire film. The SAED pattern, along [100]<sub>STO</sub> zone axis shown in Fig. 3g, confirms the nearly epitaxial growth quality of HfO<sub>2</sub> and Au with the underlying substrate as evidenced by the distinguished diffraction dots from different phases. This is consistent with the result of XRD. The EDS mapping in Fig. 3h clearly shows the distribution of Au pillars, which are uniformly embedded in both the HfO<sub>2</sub> matrix and the TiN buffer layer.

To further understand the interfacial structure of the film, high-resolution STEM was performed on the buffered HfO<sub>2</sub>-Au film. As shown in the HAADF STEM image in Fig. 4a, the Au pillars and HfO<sub>2</sub> matrix can be clearly distinguished with very different contrast considering the contrast is proportional to  $Z^{1.7}$ , i.e., brighter contrast of Au vs. lower contrast in HfO<sub>2</sub>. The diameter of the pillars is around 3 nm. The local high-resolution STEM image confirms that the lattice structure of the HfO<sub>2</sub> matrix is monoclinic, which agrees with the XRD results. It is worth noting that Au pillars in HfO<sub>2</sub> grow directly over the pillars in the TiN buffer layer, as shown in Fig. 4b. This reveals that the TiN-Au buffer layer acts as a seeding layer which improves the ordering of Au pillars.

To investigate the orientation relationship between the Au pillars and the HfO<sub>2</sub>

matrix, the plan-view TEM/STEM analysis was conducted. From the high-resolution STEM image shown in Fig. 4c, the out-of-plane growth orientation of Au is either [110] or [100], and the HfO<sub>2</sub> matrix is in [001], which matches with the XRD results. In the HfO<sub>2</sub> matrix, there are obvious domain structures exist, corresponding to 90° rotation about its [001] axis. Such rotated domain structure could help compensate the overall strain resulted from the asymmetric monoclinic structure. This also explains the high-quality epitaxial growth of the monoclinic HfO<sub>2</sub> around the cubic Au nanopillars. Further EDS mapping and line-scan analysis shown in Fig. 4d and Fig. 4e, further confirm very thin diameter of the Au pillars, ~ 3 nm, which is smaller than previously reported Au pillars in VAN structure.<sup>2, 27, 43</sup>

The laser frequency was found to play an important role in the film growth, and it can influence both pillar shape and dimension. The optimized sample shown in Fig. 3 was fabricated under the laser frequency of 2 Hz. As a comparison, a 10 Hz sample was also fabricated under the same condition, and the STEM cross-section image was shown in Fig. S3. It can be observed that some of the Au pillars can no longer grow continuously, and the pillar diameter is around 5 nm, which is much larger than that of the 2 Hz sample. This is due to the very limited diffusion time in between the pulses at 10 Hz. Therefore, suitable frequency can be key to achieve straight, continuous, ultra-fine Au pillars.

To investigate the difference between directly deposited HfO<sub>2</sub> films (fabricated by HfO<sub>2</sub> target) and the films formed by oxidation, a reference sample was fabricated with a HfO<sub>2</sub> target under the same deposition conditions as the deposition using the HfN

target. As shown in Fig. S4(a)(b), Au pillars in the directly deposited HfO<sub>2</sub> film were obviously tilted. This is likely due to the monoclinic structure of the HfO<sub>2</sub> matrix. The HfN, on the contrast, has a cubic structure, therefore the Au pillars can grow straight in the initial stage in the film growth by HfN target, and the further oxidation process convert HfN to HfO<sub>2</sub> during the remaining deposition. The high-resolution TEM image shown in Fig. S4(c) reveals that the Au pillars grows inside the monoclinic HfO<sub>2</sub> matrix by the interface steps, leading to the tilted Au pillars.

To better understand the oxidation process, a comparison sample was fabricated under room temperature. STEM images and EDS elemental mapping of this RT sample are shown in Fig. S6. It can be observed that the Au grow as nanoparticles embedded in HfN matrix under room temperature. Based on the EDS element mapping, only the very top surface portion (5 nm) of the HfN film was oxidized, and a clear contrast edge can be distinguished at the top of the HfN film in the HAADF image. This suggests that the oxidation likely happened during the cooling process after the deposition.

Since Au is embedded in the HfN matrix in the HfN-Au film, there are a lot of phase boundaries between Au and HfN, and these vertical phase boundaries can act as an oxygen diffusion path. Previous research reveals that oxygen can diffuse faster through the grain boundaries and phase boundaries.<sup>44, 45</sup> In pure HfN film, the amount of grain / phase boundaries is much less than that in the HfN-Au film. Therefore, the existence of Au nanopillars and the vertical phase boundaries could assist the oxidation process of the HfN film.

### **2.3 Optical Properties of the HfO<sub>2</sub>-Au VANs**

To investigate the optical properties of the HfO<sub>2</sub>-Au films, ellipsometry measurement was performed. The dielectric constants were fitted and presented in Fig. 5a and Fig. 5b. Due to the anisotropic structure of the film, the obtained data was modeled as in-plane ( $\epsilon^{\parallel}$ ) and out-of-plane ( $\epsilon^{\perp}$ ) components using the general oscillator models to make them Kramers–Kronig consistent. A hyperbolic region between 1050 nm and 1800 nm could be observed in the buffered HfO<sub>2</sub>-Au thin film, where the out-of-plane permittivity is negative while the in-plane permittivity is positive. The film without buffer layer shows no obvious hyperbolic region, which could be due to the random distribution of the Au pillars and particles inside the film. The anisotropic optical property makes this buffered HfO<sub>2</sub>-Au film as an ideal hyperbolic metamaterial for different optical applications.<sup>15</sup>

In addition, the transmittance measurement was also conducted for both thin films. As shown in Fig. 5c, clear absorption valleys could be observed for both thin films. In the buffered HfO<sub>2</sub>-Au thin film, only a strong adsorption peak can be distinguished at 480 nm, which results from the plasmon resonance of Au pillars. Simulated electric field maps under 480 nm incident beam by COMSOL simulation were shown in Fig. S8, which agrees well with the plasmonic resonance of Au pillars. The plasmonic resonance wavelength is much smaller than previously reported data, which is from 550 nm to 600 nm (marked as a yellow region in Fig. 5c).<sup>33, 34, 35</sup> This could be due to the low diameter of ultra-thin Au pillars, since the plasmonic absorption peak can have a redshift as the size increases.<sup>33</sup> The unbuffered HfO<sub>2</sub>-Au thin film shows two plasmonic

peaks at 480 nm and 540 nm, which could result from Au pillars and Au particles respectively. The plasmonic property could be applied in future sensor device designs.

To explore the changes of transmittance as a function of the incident angle, we have conducted angular dependent transmittance test on the buffered sample by the Lambda UV-vis system with a TAMS detector, since the Au nanowires could exhibit two plasmon resonances with different electrical field direction.<sup>46</sup> As shown in Fig. S7, the plasmon resonance peak is still around 490 nm, but more contribution from the higher wavelength region can be observed which may result from the different dimensions of Au pillars viewed from different angles. It is also noted that the plasmon resonance can be influenced by several factors, such as the matrix materials and interaction between Au pillars.<sup>47</sup> Therefore, the results of the Au pillars in HfO<sub>2</sub> could be different from the results of individual Au nanowires.

Overall, this study presents a new approach to manufacture HfO<sub>2</sub> based VAN thin films with very fine and highly aligned thin Au nanopillars. By adding suitable buffer layer, the crystallinity of the films and the nanopillar ordering were obviously improved, which indicates the importance of strain effect during the PLD growth. The as-deposited HfO<sub>2</sub>-Au thin film shows strong anisotropic optical properties, which make it as ideal as a hybrid metamaterial. However, the oxidation mechanism of HfN under HfN-Au deposition is still under investigation. HfN, deposited by itself, results in pure HfN films while the HfN-Au composite target deposition will result in the HfO<sub>2</sub>-Au films. The incorporation of Au is believed to facilitate the overall oxidation process of HfN during the growth. Further research is undergoing to explore the fundamental

mechanisms for the HfN oxidation process facilitated by the presence of Au. It is interesting to note that TiN-Au and TaN-Au VAN systems under the same growth conditions did not result in obvious oxidation issues during the composite growth, in comparison.<sup>26, 28, 48, 49</sup> Further work could focus on tuning the growth parameters for limiting oxidation process of HfN. For example, higher deposition rate and high flux of the adatoms could limit the diffusion and oxidation process as the primary nitride oxidation mechanisms have been reported based on diffusion and surface reaction.<sup>50, 51</sup> On the other hand, HfO<sub>2</sub> is also a good candidate for memristor devices, and such HfO<sub>2</sub>-Au VAN coupled in memristor designs for novel filamentary switching properties. This unique nanocomposite system could also find applications in optics, such as hyperbolic property in quantum nanophotonic application,<sup>52</sup> gain-assisted hyperlenses and tunable nonlinear imaging devices, as well as the plasmonic property in sensing device design.<sup>15</sup>

## Conclusion

In summary, self-assembled HfO<sub>2</sub>-Au nanocomposite thin films with ultra-thin Au nanopillars of 3nm has been successfully deposited on STO substrates by using a HfN target through a direct conversion process during deposition. During the PLD process, HfN was naturally oxidized to be HfO<sub>2</sub> during the co-growth of HfN-Au. The crystallinity of the film and the ordering of the Au nanopillars are improved by adding a TiN-Au buffer layer. The plasmonic resonance of the HfO<sub>2</sub>-Au VAN grown on TiN-Au buffer occurs at the wavelength around 480 nm due to the ultra-fine Au pillars.

Hyperbolic transition region of the TiN-Au buffered film ranges from 1050 nm to 1800 nm. This work paves a new way to fabricate HfO<sub>2</sub>-metal hybrid nanocomposites with strong anisotropic structure and optical properties for future optics and electronics.

## **Acknowledgement**

This work was supported by the U.S. National Science Foundation DMR-2016453 and DMR-1565822 (VAN thin film growth and High-resolution STEM work). The microscopy work was partially supported by the Laboratory Directed Research and Development program at Sandia National Laboratories. Sandia National Laboratories is a multi-mission laboratory managed and operated by National Technology and Engineering Solutions of Sandia, LLC., a wholly owned subsidiary of Honeywell International, Inc., for the U.S. Department of Energy's National Nuclear Security Administration under Contract No. DE-NA0003525. This paper describes objective technical results and analysis. Any subjective views or opinions that might be expressed in the paper do not necessarily represent the views of the U.S. Department of Energy or the United States Government.

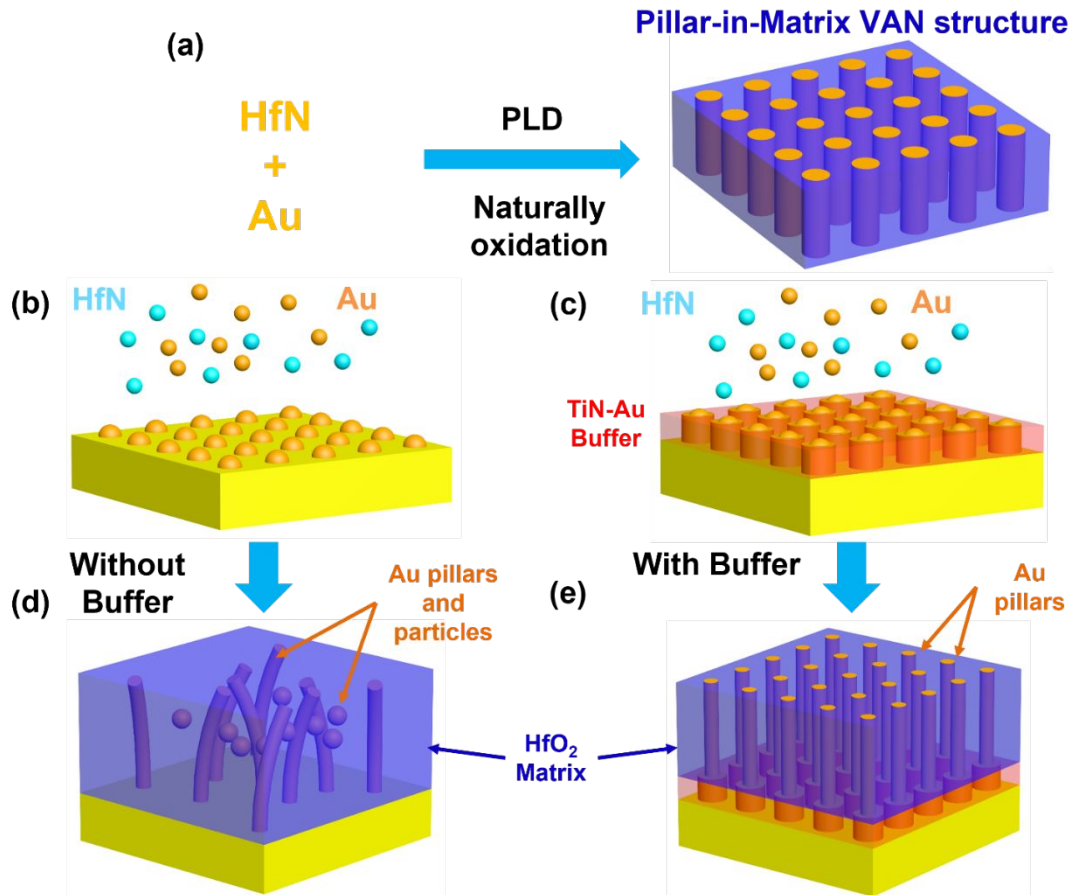


**Fig. 1** Schematic of experiments design: (a) Schematic of HfO<sub>2</sub>-Au VAN structure designed, and (b, c, d, e) schematics showing crystallinity and orientations of the films deposited with and without TiN-Au buffer.



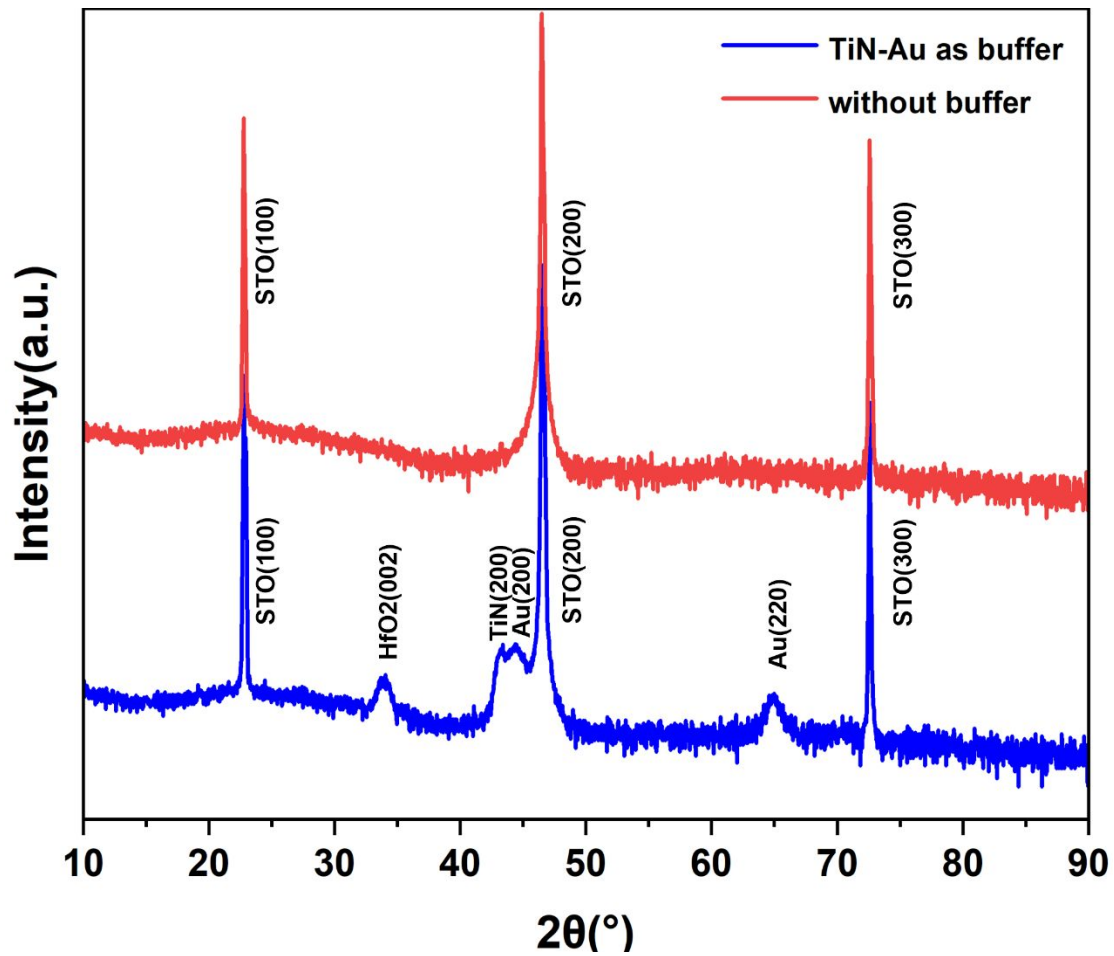


**Fig. 2** XRD  $\theta$ – $2\theta$  pattern of  $\text{HfO}_2$ -Au thin films grown on  $\text{SrTiO}_3$  (STO) (001) with or without TiN-Au buffer layer.

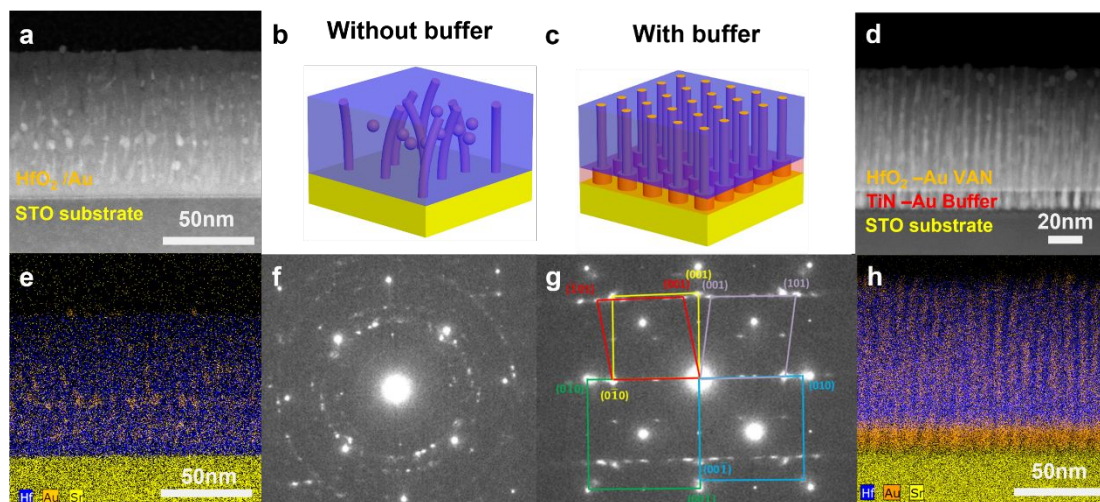


**Fig. 3** Cross-section of  $\text{HfO}_2$ -Au thin film on STO with and without TiN-Au buffer. (b,c) Schematic of the structures with and without TiN-Au buffer, (a,d) HAADF-STEM images of two films, (f,g) corresponding diffraction patterns, and (e,h) EDS element maps.

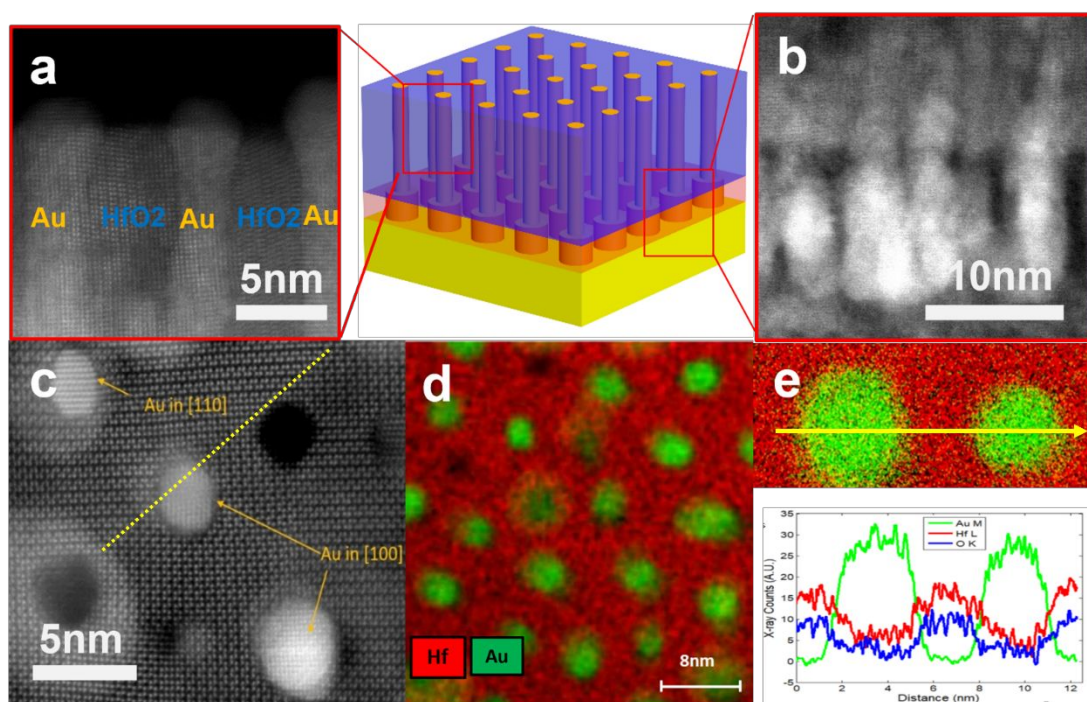


**Fig. 4** STEM cross-section and plan-view observation of HfO<sub>2</sub>-Au thin film on STO with the TiN-Au buffer. (a) cross-section image at top surface, (b) cross-section image at the interface between TiN buffer layer and HfO<sub>2</sub> film, (c) plan-view image of the film tilted to HfO<sub>2</sub> [001] projection, (d) EDS element maps of the film in the plan view (Hf-red, Au-green), and (e) EDS element maps along with the EDS line profiles across two Au columns. The yellow dash-line in (c) indicates a domain boundary position.

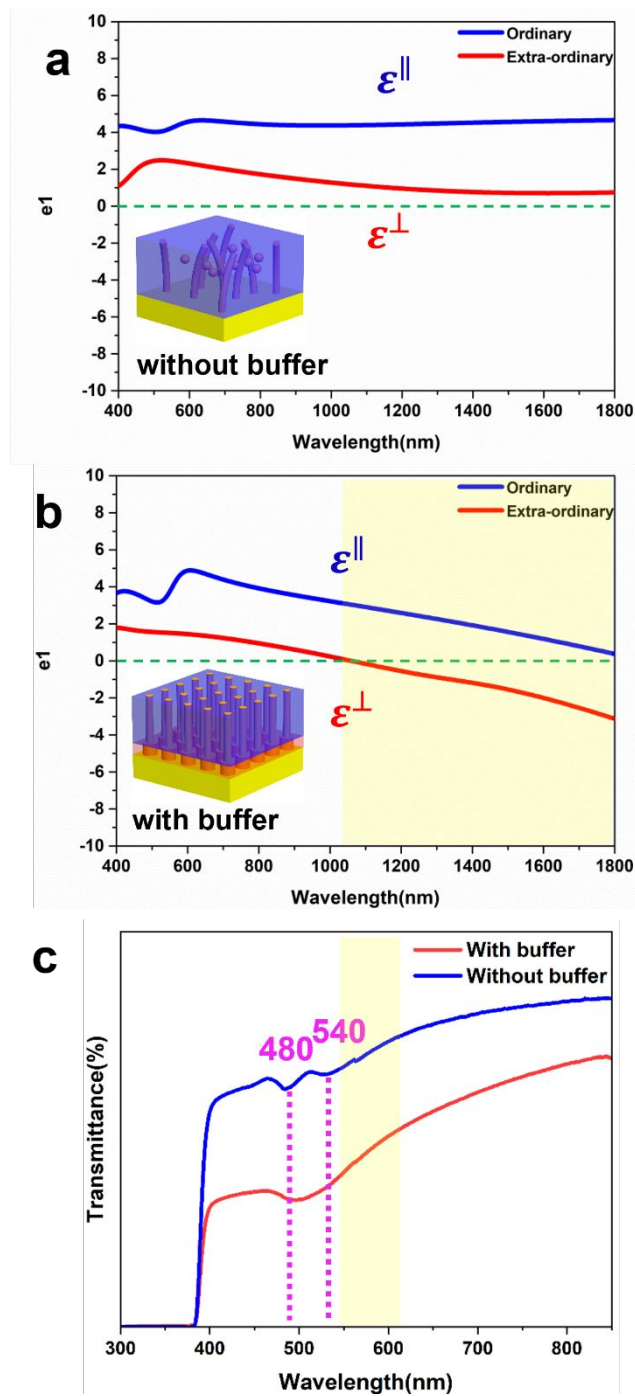


**Fig. 5** Optical properties. Dielectric constant  $\epsilon_1$  of HfO<sub>2</sub>-Au film (a) without buffer and (b) with buffer. (c) The transmittance of HfO<sub>2</sub>-Au on STO (001) with and without TiN-Au buffer.

## References

1. Zhang D, Wang H. Self - Assembled Metal - Dielectric Hybrid Metamaterials in Vertically Aligned Nanocomposite Form with Tailorable Optical Properties and Coupled Multifunctionalities. *Advanced Photonics Research* 2021, **2**(5): 2000174.
2. Zhang D, Misra S, Li L, Wang X, Jian J, Lu P, *et al.* Tunable Optical Properties in Self - Assembled Oxide - Metal Hybrid Thin Films via Au - Phase Geometry Control: From Nanopillars to Nanodisks. *Advanced Optical Materials* 2020, **8**(4): 1901359.
3. Zhang D, Lu P, Misra S, Wissel A, He Z, Qi Z, *et al.* Design of 3D Oxide - Metal Hybrid Metamaterial for Tailorable Light - Matter Interactions in Visible and Near - Infrared Region. *Advanced Optical Materials* 2021, **9**(1): 2001154.
4. Cai W, Chettiar UK, Kildishev AV, Shalaev VM. Optical cloaking with metamaterials. *Nature photonics* 2007, **1**(4): 224-227.
5. Ray C, Pal T. Retracted Article: Recent advances of metal-metal oxide nanocomposites and their tailored nanostructures in numerous catalytic applications. *Journal of Materials Chemistry A* 2017, **5**(20): 9465-9487.
6. Cargnello M, Grzelczak M, Rodríguez-González B, Syrgiannis Z, Bakhmutsky K, La Parola V, *et al.* Multiwalled carbon nanotubes drive the activity of metal@ oxide core-shell catalysts in modular nanocomposites. *Journal of the American Chemical Society* 2012, **134**(28): 11760-11766.
7. Huang J, Wang H, Qi Z, Lu P, Zhang D, Zhang B, *et al.* Multifunctional Metal-Oxide Nanocomposite Thin Film with Plasmonic Au Nanopillars Embedded in Magnetic La<sub>0.67</sub>Sr<sub>0.33</sub>MnO<sub>3</sub> Matrix. *Nano Letters* 2021, **21**(2): 1032-1039.
8. Rai P, Majhi SM, Yu Y-T, Lee J-H. Noble metal@ metal oxide semiconductor core@ shell nano-architectures as a new platform for gas sensor applications. *RSC advances* 2015, **5**(93): 76229-76248.
9. Zheludev NI, Kivshar YS. From metamaterials to metadevices. *Nature materials* 2012, **11**(11): 917-924.
10. Hess O, Pendry JB, Maier SA, Oulton RF, Hamm JM, Tsakmakidis KL. Active nanoplasmonic metamaterials. *Nature materials* 2012, **11**(7): 573-584.
11. Smith D, Schurig D. Electromagnetic wave propagation in media with indefinite permittivity and permeability tensors. *Physical Review Letters* 2003, **90**(7): 077405.
12. Li J, Fok L, Yin X, Bartal G, Zhang X. Experimental demonstration of an acoustic magnifying

- hyperlens. *Nature materials* 2009, **8**(12): 931-934.
13. Yao J, Liu Z, Liu Y, Wang Y, Sun C, Bartal G, *et al.* Optical negative refraction in bulk metamaterials of nanowires. *Science* 2008, **321**(5891): 930-930.
  14. High AA, Devlin RC, Dibos A, Polking M, Wild DS, Perczel J, *et al.* Visible-frequency hyperbolic metasurface. *Nature* 2015, **522**(7555): 192-196.
  15. Poddubny A, Iorsh I, Belov P, Kivshar Y. Hyperbolic metamaterials. *Nature photonics* 2013, **7**(12): 948-957.
  16. Mock JJ, Smith DR, Schultz S. Local refractive index dependence of plasmon resonance spectra from individual nanoparticles. *Nano letters* 2003, **3**(4): 485-491.
  17. Liu N, Guo H, Fu L, Kaiser S, Schweizer H, Giessen H. Three-dimensional photonic metamaterials at optical frequencies. *Nature materials* 2008, **7**(1): 31-37.
  18. Burckel DB, Wendt JR, Ten Eyck GA, Ginn JC, Ellis AR, Brener I, *et al.* Micrometer - scale cubic unit cell 3D metamaterial layers. *Advanced Materials* 2010, **22**(44): 5053-5057.
  19. Murdoch M, Waterhouse G, Nadeem M, Metson J, Keane M, Howe R, *et al.* The effect of gold loading and particle size on photocatalytic hydrogen production from ethanol over Au/TiO<sub>2</sub> nanoparticles. *Nature chemistry* 2011, **3**(6): 489-492.
  20. Damato TC, de Oliveira CC, Ando RA, Camargo PH. A facile approach to TiO<sub>2</sub> colloidal spheres decorated with Au nanoparticles displaying well-defined sizes and uniform dispersion. *Langmuir* 2013, **29**(5): 1642-1649.
  21. Zhou KL, Wang Z, Han CB, Ke X, Wang C, Jin Y, *et al.* Platinum single-atom catalyst coupled with transition metal/metal oxide heterostructure for accelerating alkaline hydrogen evolution reaction. *Nature Communications* 2021, **12**(1): 1-10.
  22. Barreca D, Carraro G, Comini E, Gasparotto A, Maccato C, Sada C, *et al.* Novel synthesis and gas sensing performances of CuO–TiO<sub>2</sub> nanocomposites functionalized with Au nanoparticles. *The Journal of Physical Chemistry C* 2011, **115**(21): 10510-10517.
  23. Honciuc A, Laurin M, Albu S, Sobota M, Schmuki P, Libuda J. Controlling the adsorption kinetics via nanostructuring: Pd nanoparticles on TiO<sub>2</sub> nanotubes. *Langmuir* 2010, **26**(17): 14014-14023.
  24. Huang J, Zhang D, Liu J, Wang H. Freestanding La<sub>0.7</sub>Sr<sub>0.3</sub>MnO<sub>3</sub>: NiO vertically aligned nanocomposite thin films for flexible perpendicular interfacial exchange coupling. *Materials Research Letters* 2022, **10**(4): 287-294.

25. Wang X, Jian J, Wang H, Liu J, Pachaury Y, Lu P, *et al.* Nitride - Oxide - Metal Heterostructure with Self - Assembled Core - Shell Nanopillar Arrays: Effect of Ordering on Magneto - Optical Properties. *Small* 2021, **17**(5): 2007222.
26. Wang X, Jian J, Diaz-Amaya S, Kumah CE, Lu P, Huang J, *et al.* Hybrid plasmonic Au-TiN vertically aligned nanocomposites: a nanoscale platform towards tunable optical sensing. *Nanoscale Advances* 2019, **1**(3): 1045-1054.
27. Liu J, Wang X, Gao X, Wang H, Jian J, Huang J, *et al.* Multifunctional self-assembled BaTiO<sub>3</sub>-Au nanocomposite thin films on flexible mica substrates with tunable optical properties. *Applied Materials Today* 2020, **21**: 100856.
28. Huang J, Wang X, Li D, Jin T, Lu P, Zhang D, *et al.* 3D hybrid plasmonic framework with Au nanopillars embedded in nitride multilayers integrated on Si. *Advanced Materials Interfaces* 2020, **7**(17): 2000493.
29. Chen A, Bi Z, Hazariwala H, Zhang X, Su Q, Chen L, *et al.* Microstructure, magnetic, and low-field magnetotransport properties of self-assembled (La<sub>0.7</sub>Sr<sub>0.3</sub>MnO<sub>3</sub>)<sub>0.5</sub>:(CeO<sub>2</sub>)<sub>0.5</sub> vertically aligned nanocomposite thin films. *Nanotechnology* 2011, **22**(31): 315712.
30. Lee OJ, Misra S, Wang H, MacManus-Driscoll J. Ferroelectric/multiferroic self-assembled vertically aligned nanocomposites: Current and future status. *APL Materials* 2021, **9**(3): 030904.
31. Kalaswad M, Zhang D, Gao X, Contreras LL, Wang H, Wang X, *et al.* Integration of Hybrid Plasmonic Au-BaTiO<sub>3</sub> Metamaterial on Silicon Substrates. *ACS Applied Materials & Interfaces* 2019, **11**(48): 45199-45206.
32. Huang J, Wang X, Phuah XL, Lu P, Qi Z, Wang H. Plasmonic Cu nanostructures in ZnO as hyperbolic metamaterial thin films. *Materials Today Nano* 2019, **8**: 100052.
33. Huang J, Jin T, Misra S, Wang H, Qi Z, Dai Y, *et al.* Tailorable optical response of Au-LiNbO<sub>3</sub> hybrid metamaterial thin films for optical waveguide applications. *Advanced Optical Materials* 2018, **6**(19): 1800510.
34. Misra S, Li L, Zhang D, Jian J, Qi Z, Fan M, *et al.* Self - Assembled Ordered Three - Phase Au - BaTiO<sub>3</sub> - ZnO Vertically Aligned Nanocomposites Achieved by a Templating Method. *Advanced Materials* 2019, **31**(7): 1806529.
35. Zhang D, Qi Z, Jian J, Huang J, Phuah XL, Zhang X, *et al.* Thermally Stable Au-BaTiO<sub>3</sub> Nanoscale Hybrid Metamaterial for High-Temperature Plasmonic Applications. *ACS Applied Nano Materials* 2020, **3**(2): 1431-1437.
36. Paldi RL, Sun X, Phuah XL, Lu J, Zhang X, Siddiqui A, *et al.* Deposition pressure-induced

- microstructure control and plasmonic property tuning in hybrid ZnO–Ag x Au 1– x thin films. *Nanoscale Advances* 2021, **3**(10): 2870-2878.
37. Zhang D, Misra S, Jian J, Lu P, Li L, Wissel A, *et al.* Self-Assembled BaTiO<sub>3</sub>–Au x Ag<sub>1–x</sub> Low-Loss Hybrid Plasmonic Metamaterials with an Ordered “Nano-Domino-like” Microstructure. *ACS Applied Materials & Interfaces* 2021, **13**(4): 5390-5398.
  38. Paldi RL, Lu J, Pachaury Y, He Z, Bhatt NA, Zhang X, *et al.* ZnO–Au x Cu<sub>1–x</sub> Alloy and ZnO–Au x Al<sub>1–x</sub> Alloy Vertically Aligned Nanocomposites for Low-Loss Plasmonic Metamaterials. *Molecules* 2022, **27**(6): 1785.
  39. Huang J, Phuah XL, McClintock LM, Padmanabhan P, Vikrant K, Wang H, *et al.* Core-shell metallic alloy nanopillars-in-dielectric hybrid metamaterials with magneto-plasmonic coupling. *Materials Today* 2021, **51**: 39-47.
  40. Khoshman JM, Kordesch ME. Optical properties of a-HfO<sub>2</sub> thin films. *Surface and Coatings Technology* 2006, **201**(6): 3530-3535.
  41. Tan T, Liu Z, Lu H, Liu W, Tian H. Structure and optical properties of HfO<sub>2</sub> thin films on silicon after rapid thermal annealing. *Optical Materials* 2010, **32**(3): 432-435.
  42. Fadel M, Azim M O, Omer O, Basily R. A study of some optical properties of hafnium dioxide (HfO<sub>2</sub>) thin films and their applications. *Applied Physics A* 1998, **66**(3): 335-343.
  43. Li L, Sun L, Gomez-Diaz JS, Hogan NL, Lu P, Khatkhatay F, *et al.* Self-assembled epitaxial Au–Oxide vertically aligned nanocomposites for nanoscale metamaterials. *Nano letters* 2016, **16**(6): 3936-3943.
  44. Hoffman R, Turnbull D. Lattice and grain boundary self - diffusion in silver. *Journal of Applied Physics* 1951, **22**(5): 634-639.
  45. De Souza RA, Pietrowski MJ, Anselmi-Tamburini U, Kim S, Munir ZA, Martin M. Oxygen diffusion in nanocrystalline yttria-stabilized zirconia: the effect of grain boundaries. *Physical Chemistry Chemical Physics* 2008, **10**(15): 2067-2072.
  46. Xu Q, Bao J, Capasso F, Whitesides GM. Surface plasmon resonances of free - standing gold nanowires fabricated by nanoskiving. *Angewandte Chemie International Edition* 2006, **45**(22): 3631-3635.
  47. Amendola V, Pilot R, Frascioni M, Maragò OM, Iatì MA. Surface plasmon resonance in gold nanoparticles: a review. *Journal of Physics: Condensed Matter* 2017, **29**(20): 203002.
  48. Wang X, Choi J, Liu J, Malis O, Li X, Bermel P, *et al.* 3D Hybrid Trilayer Heterostructure: Tunable Au Nanorods and Optical Properties. *ACS Applied Materials & Interfaces* 2020, **12**(40): 45015-

45022.

49. Huang J, Wang X, Hogan NL, Wu S, Lu P, Fan Z, *et al.* Nanoscale artificial plasmonic lattice in self - assembled vertically aligned nitride – metal hybrid metamaterials. *Advanced science* 2018, **5**(7): 1800416.
50. Zakutayev A, Perkins CL. Influence of protection layers on thermal stability of nitride thin films. *physica status solidi (RRL)–Rapid Research Letters* 2021, **15**(8): 2100178.
51. Harrison RW, Lee WE. Mechanism and kinetics of oxidation of ZrN ceramics. *Journal of the American Ceramic Society* 2015, **98**(7): 2205-2213.
52. Cortes C, Newman W, Molesky S, Jacob Z. Quantum nanophotonics using hyperbolic metamaterials. *Journal of Optics* 2012, **14**(6): 063001.